

# A model solid-state structural transformation: Tetragonal to Orthorhombic

Madan Rao<sup>1</sup> and Surajit Sengupta<sup>2</sup>

<sup>1</sup> *Raman Research Institute, C. V. Raman Avenue, Sadashivanagar, Bangalore 560080, India*

<sup>2</sup> *Satyendra Nath Bose National Center for Basic Sciences, Block J D, Sector III, Salt Lake, Kolkata 700098, India*

(February 7, 2020)

## Abstract

We study equilibrium properties of a system of particles in two dimensions, interacting with pair and three body potentials, which undergoes a structural transition from a square to a rhombic lattice and thus constitutes a simple model for a generic tetragonal to orthorhombic transition. We aim at an intermediate level of description lying in-between that of coarse grained elastic strain hamiltonians and microscopic ab-initio approaches. Macroscopic thermodynamic properties and phase diagram at zero and finite temperatures as a function of the density and the relative strengths of the pair and three body energies are obtained using lattice sums, an approximate ‘cell-model’ theory and molecular dynamics simulations in the NVT ensemble. We propose that this model solid can be used as a test bed for studies of statics and dynamics of structural transitions.

## I. INTRODUCTION

In spite of its fundamental and technological interest, there is as yet no general theoretical framework to predict the final microstructure of a solid following changes in temperature or stress across a structural transition [1]. This is in part because most experimental studies have focussed on technologically important solids which are far-from-idealized; thus it has been difficult to isolate generic principles amidst the volume of empirical data [2,3]. Furthermore, the spatial and temporal resolution of *in-situ* experimental probes is limited; this makes it difficult to follow microstructural changes at short length and time scales. We believe progress can only be made if we (a) identify simple ‘model’ systems which would serve as an arena for detailed studies on the dynamics of structural transitions in solids and (b) develop ‘probes’ to study the dynamics and morphology changes at short scales; in other words to *follow the motion of individual atoms as the transformation proceeds*. High speed computational modelling allows one to make useful contributions to both (a) and (b). This paper concerns point (a) – we provide a model system for a simple structural transition which could serve as a test bed for future studies of statics and dynamics of structural transitions. In another paper [4] we have discussed point (b) – we have studied the dynamics

of solid state transformations in this model system by tracking individual particles as the transformation proceeds.

Our choice of the simple structural transformation, a square to a rhombic lattice in two dimensions (2-d), is motivated by two important considerations. The first is its relevance to ‘real’ solid state transformations. The square-to-rhombus transition may be regarded as a rather accurate representation [5,6] of the three dimensional tetragonal to orthorhombic (TO) transition [7] in an oriented single crystal where the strain along the third direction ( $c$  - axis) is negligible. This transition is observed in many technologically important systems [8], such as the high- $T_c$  compound  $\text{YBa}_2\text{Cu}_3\text{O}_7$ .

The second motivation is more conceptual and warrants some explanation. Following a quench across a structural transition, the atoms constituting the solid have to rearrange themselves, since the parent phase is thermodynamically unstable. Instead of moving to the new equilibrium configuration, the motion of the atoms is arrested in a final microstructure which is very far from equilibrium. The microstructures often display features at length scales ranging from  $1000\text{\AA} - 100\mu\text{m}$ , many orders larger than the lattice spacing. A more appropriate description of the dynamics at these scales is in terms of continuum degrees of freedom. It is however not clear *a priori*, what are the relevant continuum degrees of freedom, especially in situations where the solid undergoes large deformations from the parent. In most theoretical studies of this problem, the only continuum degrees of freedom relevant at these scales have been taken to be the components of the strain tensor [9,10]. However, short length scale phenomena like atomic rearrangements [11,12] are not captured by these strain-only theories and may in some cases affect the kinetics of the transformation. The only unbiased way to determine the complete set of relevant degrees of freedom in the continuum is to start from a more microscopic description and arrive at a continuum description using a coarse-graining method [13]. Such a coarse-graining program is more easily set up in the crystallographically simpler square-to-rhombus transition.

How microscopically detailed should our microscopic model solid be ? An ab-initio or semi empirical description [14] which includes electronic degrees of freedom tailor-made for a real system such as  $\text{YBa}_2\text{Cu}_3\text{O}_7$  suffers from 3 drawbacks — (i) it compromises the need for generality, (ii) it is computationally expensive and (iii) it is difficult to extrapolate to the continuum. We therefore model an *effective* Hamiltonian accurate over distances smaller than the bulk elastic correlation length but larger than the typical atomic spacing. This effective Hamiltonian, coarse-grained over the faster electronic degrees of freedom, will in general have pair and many-body interactions.

Our model system therefore consists of a set of  $N$  ‘particles’ confined in a 2-d box of volume  $V$  at a fixed temperature  $T$ . The particles interact with each other via specific two and three -body [15] interactions. While the 2-body interaction stabilizes a rhombic lattice (triangular for *isotropic* two-body potentials), the 3-body interactions have been *constructed* to favour a square lattice. Unlike in a real solid, the square to triangular transition in our model solid may be driven by *independently* (i) increasing the density, (ii) decreasing the temperature or (iii) decreasing the relative magnitude of the three-body potential. We confine ourselves here to the equilibrium aspects of this transition and postpone a detailed study of the nucleation and coarsening dynamics to a subsequent publication [4].

In the next section we introduce our model, describing the pair and three -body potentials. In Section III we present the static lattice (zero temperature) results for the energy,

stress and the elastic constants and exhibit the zero temperature phase diagram. In Section IV we discuss the effect of finite temperatures. We present results both from a “cell model” approximation [16,17] and from molecular dynamics simulations [18] in the NVT ensemble. In Section V we discuss a simple generalization of the model to include a molecular solid with a complex basis motif. Section VI presents a summary and conclusion of this work.

## II. THE MODEL POTENTIAL

In this section we motivate the form of the *effective* hamiltonian, coarse-grained over the faster electronic degrees of freedom. Instead of starting out *ab-initio*, we shall assume that the solid can be described by a general functional of the densities of particles. A simple form of the density functional, proposed by Ramakrishnan and Yussouff (RY) [21], views the solid as an extremely inhomogeneous liquid with a non-uniform, periodic, coarse-grained density  $\rho(\mathbf{r})$ . The advantage of this approach is that it allows us to make accurate statements at any finite temperature  $k_B T = \beta^{-1}$ . Following RY, we may write the Helmholtz free energy  $F_s$  per unit volume  $V$  of the solid as,

$$\begin{aligned} \frac{\beta F_s}{V} = & \frac{1}{v} \int_v d^3 r \left[ \rho(\mathbf{r}) \ln(\rho(\mathbf{r})/\rho_s) - \rho_s \right] \\ & - \frac{1}{2} \sum_{\mathbf{G}} \rho_{\mathbf{G}} \rho_{-\mathbf{G}} C^{(2)}(\mathbf{G}) - \frac{1}{3} \sum_{\mathbf{G}_1, \mathbf{G}_2} \\ & \rho_{\mathbf{G}_1} \rho_{\mathbf{G}_2} \rho_{-\mathbf{G}_1 - \mathbf{G}_2} C^{(3)}(\mathbf{G}_1, \mathbf{G}_2, -\mathbf{G}_1 - \mathbf{G}_2) + \dots \end{aligned} \quad (1)$$

The leading term gives the ideal gas contribution (the integral is over the Wigner-Seitz unit cell of volume  $v$ ), while the subsequent terms arise from the interactions between density waves  $\rho_{\mathbf{G}}$  with wave-vector  $\mathbf{G}$  belonging to the set  $\{\mathbf{G}\}$  of reciprocal lattice vectors (RLV) of the crystalline solid. Note that we have defined the Fourier transform as,

$$\rho_{\mathbf{G}} = \frac{1}{v} \int_v d^3 r e^{i\mathbf{G}\cdot\mathbf{r}} \rho(\mathbf{r}). \quad (2)$$

The interaction terms involve the Fourier transform of the  $n^{\text{th}}$ -order direct correlation functions  $C^{(n)}(\mathbf{G}_1, \mathbf{G}_2, \dots, \mathbf{G}_{n-1})$ . These functions may either be evaluated from a liquid state theory [22] or deduced from scattering experiments (for instance,  $C^{(2)}(q) = 1 - \rho_{q=0}/S(q)$ , where  $S(q)$  is the structure factor of the liquid at wavenumber  $q$ ); however evaluation (or measurement) of direct correlation functions beyond the second order is extremely difficult [23]. Approximate ways of incorporating the effects of these higher order correlations have been used with varying degrees of success [24], though often a simple weak coupling (mean-field) approximation,  $C^{(n)} = V^{(n)}/k_B T$ , where  $V^{(n)}$  is the  $n$ -body potential, works remarkably well [25].

While the ideal gas term always prefers a uniform liquid, the sign of the interaction term decides whether the interactions stabilize (destabilize) density waves with wave-vectors  $\mathbf{G} \neq 0$ . As an example, let us consider first the effect of only the second order terms in Eq. 1. The coefficients,  $C^{(2)}(|\mathbf{G}|)$ , measure the stability of a density wave with wavenumber  $|\mathbf{G}|$ . In Fig. VIII we have plotted  $C^{(2)}(q)$  against  $q$  for a slightly supercooled hard disk liquid

[26] in two-dimensions. This function is oscillatory and has a primary peak at roughly the wave number corresponding to the magnitude of the smallest RLV of the thermodynamically stable solid. Choosing the lattice parameter such that the smallest RLV coincides with the first peak of  $C^{(2)}(q)$ , we have plotted the positions of the RLVs for the triangular (top) and square (bottom) lattices in Fig. VIII. Closed packed lattices have RLVs which are, on an average, more widely separated than those of an open lattice. As a consequence, open lattices often have RLVs lying in the region of the first *minimum* of  $C^{(2)}(q)$  which is negative, thereby contributing to a destabilisation of the lattice. From Fig. VIII we observe that this is indeed the case for the square lattice in two-dimensions [27]. Density waves corresponding to the second RLV of the square lattice with Miller index  $\{11\}$  are not favoured, making the square lattice unstable in two-dimensions.

Note that the discussion above is the finite  $T$  generalisation of the zero temperature result that for isotropic, purely repulsive *pair* potentials in two dimensions, one can only stabilize the close-packed triangular lattice [19]. For instance, a static calculation [20] of the  $T = 0$  elastic moduli of the square lattice reveals a shear instability which spontaneously distorts the lattice till it regains a close-packed structure.

In order to stabilize the square lattice one needs to go beyond the second order contribution and consider the effect of three-body correlations. As is clear from Eq. 1, a positive (and large enough !) contribution from  $C^{(3)}(\mathbf{G}_1, \mathbf{G}_2, -\mathbf{G}_1 - \mathbf{G}_2)\rho(\mathbf{G}_1)\rho(\mathbf{G}_2)\rho(-\mathbf{G}_1 - \mathbf{G}_2)$ , where any one (or two) of the wave-vectors equals  $\{11\}$ , can compensate for the destabilizing effect of the second order correlator [27]. There are many choices for the wave-vectors  $\mathbf{G}$ , but the simplest combination is  $\mathbf{G}_1 = \mathbf{G}_2 = \{10\}$  (so that  $\{10\} + \{01\} = \{11\}$ ). A straightforward way to ensure that this combination of density waves is stabilized is to stabilize the *real space* triangle involving the direct lattice vectors (10), (01) and (11) (and those related to them by symmetry). Within a simple minded mean-field approximation this may be accomplished, as shown below, by choosing an appropriate three-body potential which favours  $0^\circ$ ,  $45^\circ$  and  $90^\circ$  bonds. Higher-order interactions involving four or more particles, though present in principle, are not necessary for our purpose.

Our model system, constructed from this level of coarse-graining, therefore consists of ‘point-particles’ interacting with effective pair and three-body potentials. The interaction energy  $E$  of the system is given by,

$$E = \frac{1}{2} \sum_{i \neq j} \Psi_2(\mathbf{r}_{ij}) + \frac{1}{6} \sum_{i \neq j \neq k} \Psi_3(\mathbf{r}_{ij}, \mathbf{r}_{jk}, \mathbf{r}_{ki}). \quad (3)$$

For the pair potential we take,

$$\Psi_2(|\mathbf{r}_{ij}|) = V_2 \left( \frac{\sigma}{|\mathbf{r}_{ij}|} \right)^{12}, \quad (4)$$

which is purely repulsive and therefore the system has to be confined with a uniform hydrostatic pressure (see below). A purely repulsive system simplifies our analysis since there is one fewer length scale and one fewer non-solid phase. Without the 3-body potential, our system is characterized by only one parameter instead of the two (temperature and density). On including the 3-body potential, we lose this simplification, but the variation of thermodynamic properties with density is still weak. Without loss of generality we can take  $V_2$  and  $\sigma$  to be our units for energy and distance respectively.

The 3-body potential is

$$\begin{aligned} \Psi_3(\mathbf{r}_{ij}, \mathbf{r}_{jk}, \mathbf{r}_{ki}) = V_3 \left[ \right. & f_{ij} \sin^2(4\Theta_i) f_{ik} \\ & + f_{ij} \sin^2(4\Theta_j) f_{jk} \\ & \left. + f_{jk} \sin^2(4\Theta_k) f_{ki} \right] \end{aligned} \quad (5)$$

where the function,

$$\begin{aligned} f_{ij} \equiv f(r_{ij}) &= (r_{ij} - r_0)^2 & r_{ij} < r_0 \\ &= 0 & \text{otherwise} \end{aligned} \quad (6)$$

and we have used the notation  $r_{ij} \equiv |\mathbf{r}_{ij}|$ . The angles are as defined in Fig. 2. The function  $f_{ij}$  provides a cutoff for the 3-body potential; as long as  $f_{ij}$  is short ranged, the actual form of this function does not affect the qualitative results.

It may appear that a three-body potential requires a large investment in terms of computer times. This apprehension is fortunately unfounded. The form of this potential ensures that three-body energies can be calculated [15] extremely efficiently, requiring a computational effort not exceeding that for the pair part. This is discussed in the Appendix.

### III. ZERO TEMPERATURE RESULTS

At zero temperature, the equilibrium configuration is a solid which minimises the potential  $E$ . Since we work in the constant NVT (and shape) ensemble, the density  $\rho = N/V$  is a constant. Assuming that the only minima of  $E$  correspond to the triangular or square phases, we have numerically deduced the  $T = 0$  phase diagram in the  $\rho - V_3$  plane (Fig. 3). Later in this section we show, within a restricted variational calculation, that these are the only minimisers of  $E$ . As we see from Fig. 3, the triangular lattice is the lowest energy phase at high densities and small values of  $V_3$ , *i.e.*, wherever the pair interaction dominates over the three-body part. Across the boundary there is a strong first-order transition with a discontinuous change in the slope  $(\partial E / \partial \rho)_{V_3}$ .

To deduce the nature of the order parameter distinguishing the square from the triangular phase, we look at how a rhombic lattice may be obtained from a square. Such an analysis makes contact with continuum elasticity in a natural way.

At zero temperature, a continuous family of perfect rhombic lattices (labelled by position vectors  $\mathbf{R}^T$ ) can be obtained from the perfect square lattice (labelled by  $\mathbf{R}^0$ ) by the transformation,  $\mathbf{R}^T = (\mathbf{I} + \mathbb{T})\mathbf{R}^0$  where the transformation matrix  $\mathbb{T}$  is,

$$\mathbb{T} = \begin{pmatrix} \epsilon_1/2 + \epsilon_2/2 & \epsilon_3 \\ \epsilon_3 & \epsilon_1/2 - \epsilon_2/2 \end{pmatrix}. \quad (7)$$

The parameters  $\epsilon_\alpha$  ( $\alpha = 1, 2, 3$ ) are related to the components of a strain tensor by the following construction. We choose to measure all distortions and energies with respect to the undistorted *square* phase — our reference state. The microscopic displacements  $\mathbf{u}_{\mathbf{R}^0} = \mathbf{R}^T - \mathbf{R}^0$  are therefore defined at every  $\mathbf{R}^0$  on the reference lattice, *i.e.*, we use *Lagrangian* [19,28] coordinates. The full nonlinear Lagrangian strain tensor [28]  $\epsilon_{ij}$  is,

$$\epsilon_{ij} = \frac{1}{2} \left( \frac{\partial u_i}{\partial r_j} + \frac{\partial u_j}{\partial r_i} + \frac{\partial u_k}{\partial r_i} \frac{\partial u_k}{\partial r_j} \right), \quad (8)$$

where the indices  $i, j$  go over  $x$  and  $y$ . The parameters  $\epsilon_\alpha$  in Eq. 7 represent the combinations  $\epsilon_{xx} + \epsilon_{yy}$ ,  $\epsilon_{xx} - \epsilon_{yy}$  and  $\epsilon_{xy}$  respectively, which reduce to the usual volumetric, deviatoric and shear strains once nonlinearities are neglected. Note that one may start with a prescribed square and end with a final triangular lattice in more than one way — the transformation parameters are not unique. For instance, for a given orientation of the parent square lattice shown in Fig. 4(i) one obtains a rhombic lattice using  $\epsilon_2 = 0$  and  $\tan \theta = \epsilon_3/(1 + \epsilon_1)$ . Equivalently (Fig. 4(ii)) the square lattice (first rotated by  $45^\circ$ ) can be transformed to a centered rectangular lattice with  $\epsilon_3 = 0$  and  $b/a = (1 + \epsilon_2 + \epsilon_1/2)/(1 - \epsilon_2 + \epsilon_1/2)$ . The two transformations are completely equivalent.

One of the offshoots of this nonuniqueness, is that any rhombus obtained as a uniform deformation of a perfect square, can be represented by two independent parameters  $\epsilon_1$  and  $\epsilon_3$ . In addition, since the density  $\rho$  is a constant in our NVT ensemble,  $\epsilon_1$  is related to  $\epsilon_3$ ;  $\epsilon_1 = \sqrt{1 + \epsilon_3^2} - 1 \approx \epsilon_3^2/2$ . Thus all rhombic lattices considered by us can be labelled by a single parameter  $\epsilon_3 = \epsilon$  (which by definition is 0 for the perfect square lattice). This makes the shear strain  $\epsilon$  a good order parameter which distinguishes the square from the triangular lattices.

We may now calculate the energy of  $T = 0$  configurations as a function of the order parameter  $\epsilon$ . A calculation of the energy  $E$  and its derivatives (elastic moduli) for a given lattice involves computation of lattice sums. We start with a finite square lattice containing  $10 \times 10$  sites and allow the transformation  $\mathbb{T}$  to produce a continuous sequence of rhombic lattices labelled by  $\epsilon$ . We have checked for convergence of the lattice sums by increasing the size of the lattice and observing the consequent change in the numerical values. In Fig. 5 we have plotted the energy per particle  $E/N$  as a function of the parameter  $\epsilon$  for various values of  $V_3$  (keeping  $\rho$  fixed). Note that for large values of  $V_3$  there is only one minimum at  $\epsilon = 0$  so that the square lattice is the only stable phase. For smaller values of  $V_3$  two additional degenerate minima appear at  $\epsilon = \pm\epsilon_0 = \pm 0.27812$  which correspond to the triangular lattice. The transition is first-order with the order parameter jumping discontinuously,  $|\Delta\epsilon| = \epsilon_0$ . Note that in this model the change in the shear strain across the transition is fixed; we shall return to this point in Sect. V where we propose a variant of this model in which the jump in the shear strain across the structural transition can be made arbitrarily small. As expected, the square and triangular lattices are the only minimisers of  $E$  within this parametrisation scheme.

To make contact with elasticity theory we may compute stresses and elastic moduli, obtained by evaluating appropriate derivatives of the energy keeping  $T, N, V$  constant —  $\partial E/\partial\epsilon_\alpha = \sigma_\alpha$  (Fig. 6), and  $\partial^2 E/\partial\epsilon_\alpha\partial\epsilon_\beta = C_{\alpha\beta}$  (Fig. 7). Note that our system is always under a hydrostatic pressure  $P = \sigma_1$ ; the constant density constraint implies that for  $\epsilon \neq 0$  there is an applied shear stress  $\sigma_3 = P(\epsilon)\epsilon$  (Fig. 6). This implies that the slope of the shear stress *vs*  $\epsilon_3$  curve is not the shear modulus  $C_{33}$  (defined for zero external stress) but  $C_{33} + P$  (Fig. 7).

At this stage, we find it useful to point out that the results of Figs. 5-7 can be rationalized using a systematic power series expansion of the energy in terms of  $\epsilon_\alpha$ . Although such expansions are quite common in the literature [5,10], our results show that fourth order terms in  $\epsilon_\alpha$ , especially cross couplings of the form  $\epsilon_1^2\epsilon_3^2$  and  $\epsilon_2^2\epsilon_3^2$ , together with coupling to

the external hydrostatic pressure  $P$  need to be included in order to reproduce the  $T = 0$  results accurately. The coefficients of all these terms are however not independent. For instance, relationships like,

$$\left. \frac{\partial^2 F}{\partial \epsilon_2^2} \right|_{\epsilon_0} = \left. \frac{\partial^2 F}{\partial \epsilon_3^2} \right|_{\epsilon_0} \quad (9)$$

dictated by the geometry of the triangular phase have to be satisfied for all temperatures and densities.

In this section we have been able to show that our model potential indeed produces the square and the triangular lattices as minima of the energy. The potential parameters maybe tuned, if necessary, to a real system by comparing the elastic properties of this model system to experimentally measured quantities. By varying the density or the strength of the three-body potential one obtains a zero temperature first order structural transition between a square and triangular lattice. What happens to the structural transition at non-zero temperatures? We study this question in the next section.

#### IV. NONZERO TEMPERATURE RESULTS

In this section we analyse the phase diagram at  $T \neq 0$  as a function of  $V_3$  or  $\rho$ . We do this by two methods — an ‘exact’ molecular dynamics (MD) simulation [18] in the constant NVT ensemble, using the 2- and 3-body potentials defined earlier, and an approximate ‘cell-model’ [16] based on the deformation parameter  $\epsilon$ . The latter leads naturally to an approximate continuum elasticity description at  $T \neq 0$ . We take up the cell-model analysis first and compare its results with the exact MD simulation in the next subsection.

##### A. Cell model approximation: free energies and phase stability

Imagine being in a region of the zero temperature parameter space  $V_3 - \rho$ , where the square solid is the stable minimum of the energy. As the temperature is gradually increased, the contribution of the phonon entropy to the (Helmholtz) free energy destabilizes the square lattice. In order to quantify this effect one needs to go beyond the static lattice and consider phonon fluctuations. Although a direct calculation of the contribution of phonons to the lattice energy is straightforward [20], we choose to use the much simpler, though not necessarily less accurate ‘cell-model’ approximation.

Before discussing the cell-model approximation, let us mark its regime of validity. First, the cell-model approximation neglects contributions from topological defects like dislocation-antidislocation pairs and thus breaks down near the melting point [13]. In two dimensions, there is a further complication, since fluctuations of the displacement field  $\mathbf{u}$  due to phonons diverge logarithmically [19] with system size. This divergence is however weak and may be ignored for the system sizes under consideration.

Recall that at  $T = 0$ , the configurations of the perfect rhombi were parametrised by a single deformation variable  $\epsilon$ . Is this true at  $T \neq 0$ , when the lattices are not perfect due to phonon fluctuations? It turns out that the constraints of rhombic symmetry and constant density still allow a parametrization of the  $T \neq 0$  configurations by a single *function*  $\epsilon(\mathbf{x})$ ,

at least when the temperatures are low. Thus the energy  $E$  may be written as a functional of  $\epsilon$ , which at low temperatures may be replaced by its mean  $\langle\epsilon\rangle$ .

Within the cell - model approximation, the partition function of a lattice of  $N$  particles at temperature  $T$  is given by [16],

$$Z(\langle\epsilon\rangle, T, N) = [\Lambda^{-3} \int_{v_\epsilon} d\mathbf{r} \exp(-\delta\phi_\epsilon(\mathbf{r})/k_B T)]^N \times \exp(-E(\langle\epsilon\rangle)/k_B T) \quad (10)$$

where  $\Lambda$  is the thermal wavelength and  $\delta\phi$  is the change in potential energy of a single particle as it moves around within a unit cell of size  $v_\epsilon$  in a potential well arising from its interaction with all its neighbours. A further harmonic approximation for  $\delta\phi$  leads to the familiar Einstein approximation. At the other extreme, for the hard disk potential,  $\delta\phi = 0$  except where overlaps occur and the cell-model approximation becomes identical to the *free volume* [17] theory. The Helmholtz free energy for any rhombic lattice labelled by  $\langle\epsilon\rangle$  may now be obtained by using  $F = -k_B T \log Z$ .

Evaluation of the Helmholtz free energy (Fig. 8) allows us to calculate the  $V_3 - T$  phase diagram at any density  $\rho$  as also the limits of metastability of the square lattice.

## B. Molecular dynamics simulations

To obtain accurate results for the phase stability at non-zero temperatures, we have used a molecular dynamics simulation for our model system. We simulate  $N = 2499$  particles ( $50 \times 50$  unit cells with vacancy to improve the kinetics) in the NVT ensemble using a standard Nosé-Hoover thermostat. Starting from an ideal square lattice, we have equilibrated systems at various values of  $V_3$  and temperature for a fixed density for about  $50 - 100 \times 10^3$  molecular dynamics time steps or till thermodynamic quantities like the pressure and energy have stabilized. The final structure is then examined and this information used to obtain the phase diagrams shown in Fig. 9. We display the phase diagram for two densities  $\rho = 1.05$  and  $1.1$ . Together with the molecular dynamics results we have also plotted the results of the cell-model approximation. We observe that for low temperatures, the cell-model approximation faithfully reproduces the actual phase boundary while at higher temperatures it begins to deviate. The cell-model approximation is also used to plot the limit of stability of the square phase in the triangular region.

Both the molecular dynamics simulations and the cell model calculations predict that the square to triangular transition remains first-order over a wide region of parameter space even at non-zero temperatures. For larger density, the transition point shifts to higher values of  $V_3$ . This is expected since a high density favours the triangular lattice. Also, the square phase becomes unstable for lower values of  $V_3$  as the density is increased. The jump in the order parameter remains fixed at  $|\Delta\epsilon| = \epsilon_0$  all along the transition line. This aspect of our model is specifically addressed in the next section, where we show that inclusion of an anisotropic *pair* interaction allows one to tune the order parameter jump all the way to zero.

We end this section with the following observations. We have seen that the exact MD and approximate cell model give qualitatively similar results. More sophisticated phonon fluctuation calculations may even produce quantitative agreement. Figure 8 suggests that the Helmholtz free energy may be expanded in powers of  $\epsilon$ , just as was noted at  $T = 0$ .



Though we do not explicitly demonstrate here, we may recover elasticity theory (including corrections arising from thermal fluctuations) by constructively coarse-graining as in Ref. [13].

## V. GENERALIZATION TO MOLECULAR SOLIDS

The model 2-d solid discussed in the preceding sections has the virtue that it is simple enough to begin a detailed theoretical study of both the equilibrium and dynamical features of the TO transition across a range of length and time scales. However if we were to compare the results of such a study with experiments on realistic systems, we would immediately face a problem. Most solids undergoing a TO transition [5,6], for instance  $\text{YBa}_2\text{Cu}_3\text{O}_7$ , have a complex basis, consisting of many atoms per unit cell. These systems generically have much smaller jumps in the shear strain at the TO transition compared to the jump computed in the previous section. To appreciate the *quantitative* discrepancy, recall the discussion following Eq. 8, where we showed that any perfect rhombus obtained as a deformation of a square may be parametrized by either  $\epsilon$  or  $b/a$ . Defining an *orthorhombic distortion* as  $D \equiv (b - a)/(b + a)$ , we find that  $D = (\sqrt{3} - 1)/(\sqrt{3} + 1) \approx 0.27$  for our model square-to-triangle structural transition – significantly larger than  $D = 0.0085$  for the TO transition in  $\text{YBa}_2\text{Cu}_3\text{O}_7$ .

Apart from this, there might be a more serious *qualitative* mismatch between our model solid and real systems undergoing a TO transition. Changes in temperature or pressure (hydrostatic or chemical) may lead to a local structural rearrangement (optical modes) which would couple to the strain tensor. The jump in the shear strain across the structural transition may therefore, unlike in our model solid, vary along the phase boundary, even going to zero (phonon softening) at a critical point [29].

We shall see that we may address both these issues within an anisotropic variant of our model solid. Our attempt will be to incorporate the complex basis, with many atoms per unit cell, into an *effective* hamiltonian between ‘point particles’. In the spirit of an effective hamiltonian, we will coarse-grain the density over a length and time scale corresponding to the ‘size’  $\xi$  and relaxation time  $\tau$  of the basis. Thus we may define a coarse-grained density as  $\rho(\mathbf{r}) = p^{-1} \sum_{\mu} \rho_{\mu}(\mathbf{r})$ , where  $\mu = 1, \dots, p$  labels the atomic species making up the basis. This coarse-grained density profile  $\rho(\mathbf{r})$  will have peaks at the centre of mass of each basis, falling off to zero over a length scale  $\xi$  and having a cross section which is spatially anisotropic. If we assume that this anisotropic cross section has a fixed shape at a given temperature and pressure (true when the associated optical branch is much higher than the acoustic branches), then we may write the effective hamiltonian as arising from a collection of ‘point particles’ interacting via an anisotropic potential. The form of the effective hamiltonian may also be motivated in terms of a density wave picture [30] in much the same way as in Section II. An anisotropic density interacts via an anisotropic direct correlation function. Within a mean field approach this reduces to a pair potential which depends not only on the distance between the two basis motifs but also on their orientation relative to the crystal axes — orientation fluctuations within the motifs being neglected.

For specificity if we assume 2 atoms per basis, we may then arrive at the following modification of the two-body potential using the arguments outlined above,

$$\Psi_2(|\mathbf{r}_{ij}|) = V_2 \left( \frac{\sigma}{|\mathbf{r}_{ij}|} \right)^{12} \times \left( 1 + \alpha \sin^2 4(\theta_{ij} - \psi) \right), \quad (11)$$

where the anisotropy parameter  $\alpha$  has a fixed value at constant  $T$  and  $P$ . On the other hand, the 3-body potential may be taken to be the same as in Eq. 5. Setting  $\gamma = 1 + \alpha$ , we see that  $\gamma$  is always positive. All angles are measured with respect to the [01] axes of the undistorted square lattice. The angle  $\psi$  represents the orientation of the basis and  $\theta_{ij} = \sin^{-1}(x_{ij}/|\mathbf{r}_{ij}|)$ , see Fig. 10. The total energy is a function of  $\psi$  so that uniform rotations of the basis with respect to the crystal axes cost energy (optical mode) while simultaneous rotations of the basis together with the crystal axes is a symmetry of the hamiltonian.

Using the modified two-body potential (Eq. 11), we compute the energy as a function of  $\epsilon$  as in Section III. For a fixed  $\alpha$ , the total energy minimized with respect to  $\psi$  and  $\epsilon$  leads to  $\psi = 0$  (independent of  $\epsilon$ ). As before there are 3 minima in  $\epsilon$ , one at  $\epsilon = 0$  (corresponding to a square) and the other two corresponding to rhombi with  $|\epsilon|$  being *smaller* than the value for the perfect triangular lattice  $\sim .28$  (Fig. 10). The jump in the value of the shear strain  $\epsilon$  across the structural transition is therefore smaller than that obtained in Section III. Moreover we find that this jump in  $\epsilon$  goes to zero and the region over which the square phase is metastable shrinks and disappears as  $V_3 \rightarrow 0$  thus indicating a *continuous transition* at a tricritical point. One expects, therefore, that for real systems fluctuation effects near the T-O transition would be more pronounced. This fact is actually borne out by experiments [5,8].

The zero and finite temperature phase diagrams are shown in Fig. 11. The zero temperature phase diagram clearly shows the location of the tricritical point where the jump in the order parameter vanishes. The effect of finite temperatures is addressed easily within a cell-model approximation. The calculation may be carried out along the lines outlined in the last section. Once again we see that the Helmholtz free energy can be written as a power series expansion in  $\epsilon$ . The results of the calculation are expected to be accurate at low temperatures if the anisotropy is not too large. For larger anisotropies the effect of (tri)-critical fluctuations may alter the results of our simple mean-field estimates. Our result shows that the square lattice now becomes stable over a much larger range of  $V_3$  than in the isotropic case. The region of metastability of the square lattice however decreases and the first-order transition is weakened.

## VI. SUMMARY AND CONCLUSION

In this paper we have described a model system which is designed to undergo a square to rhombus transition in two dimensions. We believe that our study will be useful in two ways. On the one hand, it may be used as a simple simulational model for the T-O transition in real materials which often consists of a large number of individual atomic species making it difficult to study using ab-initio methods. For this purpose, the parameters  $V_3$  and  $\alpha$  have to be “fitted” to observed properties of the particular realistic system. On the other hand, we could use this system to study, in general, the dynamical pathways of a simple first order solid state phase transition involving a structural transition. It is this context that we would like to emphasize. Once the equilibrium properties are determined, we look at the nucleation dynamics, growth modes and microstructure of the rhombic phase growing

in the matrix of the parent square lattice [4]. The effect of defects such as vacancies and dislocations are automatically incorporated in our microscopic approach. In future, we hope to obtain atomistically detailed information about the statics and dynamics of solid-solid interfaces.

## VII. ACKNOWLEDGEMENT

Discussions with S. Sastry and G. Baskaran are gratefully acknowledged. MR thanks the Department of Science and Technology for a Swarnajayanthi Fellowship.

## VIII. APPENDIX

In general, evaluation of three body energies requires sums over all possible triplets which for a system of reasonable size is prohibitively expensive. The particular form for the three body potential used by us is, however, special and can be evaluated without keeping track of triplets. We illustrate below how this may be done for our system [15,31] and derive an explicit expression for the energy.

The three body part of the energy (see Eq. (1) ) is given by,

$$\begin{aligned}
E_3 &= \frac{1}{6} \sum_{i \neq j \neq k} \Psi_3(\mathbf{r}_{ij}, \mathbf{r}_{jk}, \mathbf{r}_{ki}) \\
&= \frac{1}{2} \sum_{i \neq j \neq k} \frac{V_3}{4} f_{ij} \sin^2(4\theta_i) f_{ik} \\
&= \sum_{i \neq j \neq k} 2(\sin^2 \theta_i \cos^2 \theta_i - 4 \sin^4 \theta_i \cos^4 \theta_i) f_{ij} f_{ik}
\end{aligned} \tag{12}$$

Now define  $\tilde{x}_{ij} = x_{ij}/r_{ij}$  and  $\tilde{y}_{ij} = y_{ij}/r_{ij}$  so that  $\sin \theta_i = \tilde{x}_{ik}\tilde{y}_{ij} - \tilde{x}_{ij}\tilde{y}_{ik}$  and  $\cos \theta_i = \tilde{x}_{ik}\tilde{y}_{ij} + \tilde{x}_{ij}\tilde{y}_{ik}$ . Using the above definitions and the quantities,

$$\begin{aligned}
g_{ij}(1) &= \tilde{x}_{ij}^2 \tilde{y}_{ij}^2 f_{ij} \\
g_{ij}(2) &= \tilde{x}_{ij}^2 \tilde{y}_{ij}^2 (\tilde{x}_{ij}^2 - \tilde{y}_{ij}^2) f_{ij} \\
g_{ij}(3) &= \tilde{x}_{ij}^4 \tilde{y}_{ij}^4 f_{ij} \\
g_{ij}(4) &= \tilde{x}_{ij}^2 \tilde{y}_{ij}^2 (\tilde{x}_{ij}^2 - \tilde{y}_{ij}^2)^2 f_{ij} \\
g_{ij}(5) &= \tilde{x}_{ij}^3 \tilde{y}_{ij}^3 (\tilde{x}_{ij}^2 - \tilde{y}_{ij}^2) f_{ij}
\end{aligned} \tag{13}$$

We get,  $E_3 = V_3 \sum_i S_i$  with,

$$\begin{aligned}
S_i &= 4 [G_i(1)F_i - 4 G_i(1)^2 - G_i(2)^2] - 16 \times \\
&\quad \{G_i(3)F_i + 32 G_i(3)^2 + 2 G_i(4)^2 + G_i(1)^2 - \\
&\quad 16 G_i(3)G_i(1) - 4 G_i(5)G_i(2) + 16 G_i(5)^2\}
\end{aligned} \tag{14}$$

and  $G_i(n) = \sum_{j \neq i} g_{ij}(n)$  and  $F_i = \sum_{j \neq i} f_{ij}$ . The three body forces can be got by taking derivatives of  $E_3$  which can be cast into a similar form.

## REFERENCES

- [1] H. I. Aaronson, *The Mechanism of Phase Transformations in Crystalline Solids*, (The Institute of Metals, London, 1969); H. I. Aaronson *et. al.* (eds.) *Proc. Int. Conf. on Solid-Solid Phase Transformations*. (The Metall. Soc. AIME, New York, 1981); A. G. Kachaturyan, *The Theory of Structural Transformations in Solids* (Wiley, New York, 1983); G. B. Olson and W. S. Owen (eds.), *Martensite*, (American Society of Metals, 1992)
- [2] *Metals Handbook* (American Society of Metals, Ohio, 1973).
- [3] E. K. H. Salje, A. Buckley, G. Van Tendeloo, Y. Ishibashi and G. L. Nord Jr., *American Mineralogist* **83**, 811 (1998); G. Van Tendeloo, H. W. Zandbergen and S. Amelinckx, *Solid State Commun.* **63**, 389 (1987).
- [4] M. Rao and S. Sengupta, preprint (2001).
- [5] A. E. Jacobs, *Phys. Rev. B* **31**, 5984 (1985); S. Kartha, T. Castán, J. A. Krumhansl and J. P. Sethna, *Phys. Rev. Lett.* **67**, 3630 (1991); S. Kartha, J. A. Krumhansl, J. P. Sethna, and L. K. Wickham, *Phys. Rev. B* **52**, 803 (1995); A. Onuki, *J. Phys. Soc. Jpn.* **68**, 5 (1999); S. R. Shenoy, T. Lookman, A. Saxena and A. R. Bishop, *Phys. Rev. B* **60**, 12537 (1999); S. H. Curnoe and A. E. Jacobs, cond-mat/0012312.
- [6] R. V. Kohn and S. Müller, *Philos. Mag. A* **66**, 697 (1992).
- [7] E. K. H. Salje, *Phase Transitions in Ferroelastic and Co -elastic Crystals*, Cambridge University Press (1993).
- [8] A. H. King and Y. Zhu, *Philos. Mag. A* **67**, 1037 (1993); Y. Zhu, M. Suenaga and J. Taftø, *Philos. Mag. A* **67**, 1057 (1993); C. Chu, PhD thesis, Univ. Minnesota (1993).
- [9] M. Rasclé, D. Serre and M. Slemrod eds. *Partial Differential Equations and Continuum Models of Phase Transitions*, (Lecture Notes in Physics **344** Springer-Verlag, 51, 1989).
- [10] F. Falk, *Z. Phys. B: Condens. Matter* **51**, 177 (1983); G. R. Barsh and J. A. Krumhansl, *Phys. Rev. Lett.* **53**, 1069 (1984);
- [11] S. Semenovskaya and A. G. Kachaturyan, *Phys. Rev. Lett.* **67**, 2223 (1991); *Phys. Rev. B* **46**, 6511 (1992); S. Semenovskaya, Y. Zhu, M. Suenaga, and A. G. Khachaturyan, *Phys. Rev. B* **47** 12182 (1993).
- [12] M. Rao and S. Sengupta, *Phys. Rev. Lett.* , **78**, 2168 (1997); M. Rao and S. Sengupta, *Curr. Sci.* **77**, (1999); M. Rao and S. Sengupta, *Curr. Sc.* **77**, 382-387 (1999).
- [13] S. Sengupta, P. Nielaba, M. Rao and K. Binder, *Phys. Rev. E* **61**, 1072, (2000); S. Sengupta, P. Nielaba and K. Binder, *Phys. Rev. E* **61**, 6294, (2000).
- [14] C. S. Becquart, P. C. Clapp and J. A. Rifkin, *Phys. Rev. B* **48**, 6, (1993); R. Meyer and P. Entel, cond-mat/9706248; M. S. Daw and M. I. Baskes, *Phys. Rev. Lett.* **50**, 1285 (1983); M. S. Daw and M. I. Baskes, *Phys. Rev. B* **29**, 6443 (1984).
- [15] T. A. Weber and F. H. Stillinger, *Phys. Rev. E* **48**, 4351 (1993).
- [16] D. R. Squire, A. C. Holt and W. G. Hoover, *Physica (Utrecht)* **42**, 388 (1969).
- [17] W. G. Hoover, W. T. Ashurst and R. Grover, *J. Chem. Phys.* **57**, 1259 (1972); W. G. Hoover, N. E. Hoover and K. Hanson, *J. Chem. Phys.* **70**, 1837 (1979); W. G. Hoover and F. H. Ree, *J. Chem. Phys.* **49**, 3609 (1968).
- [18] D. Frenkel and B. Smit *Understanding Molecular Simulations* (Academic Press, San Diego, 1996).
- [19] P. M. Chaikin and T. C. Lubensky, *Principles of condensed matter physics*, (Cambridge University Press, Cambridge, 1995).

- [20] M. Born and K. Huang, *Dynamical Theory of Crystal Lattices*, (Oxford University Press, Oxford, 1998).
- [21] T. V. Ramakrishnan and M. Yussouff, Phys. Rev. B **19**, 2775 (1979).
- [22] J-P. Hansen and I. R. McDonald, *Theory of Simple Liquids*, (Academic Press, London, 1986).
- [23] See for eg. A. R. Denton and N. W. Ashcroft, Phys. Rev. A **39**, 426 (1989).
- [24] For reviews of density wave theory see eg. E. Tareyeva and V. Ryzhov cond-mat/9712265; H. Löwen, Phys. Rep. **237**, 249 (1994); *Liquids, Freezing and Glass Transition, Les Houches session 51*, J-P. Hansen, D. Levesque and J. Zinn-Justin, Eds. (North-Holland, Amsterdam, 1991).
- [25] A. R. Denton, G. Kahl and J. Hafner, J. Non-Crystalline Solids **15**, 250, (1999).
- [26] Y. Rosenfeld, Phys. Rev. A **42**, 5983 (1990).
- [27] A similar situation exists for the body centered cubic lattice in three dimensions. Second order contributions always prefer a closed packed face centered cubic structure and in order to discuss the relative stability of these two lattices three body correlations have to be invoked; S. Sengupta, Ph.D thesis, Indian Institute of Science, Bangalore (1991). For an application to the system of charged stabilized colloids, see, S. Sengupta and A. K. Sood, Phys. Rev. A **44**, 1233, (1991) N. Choudhury and S. K. Ghosh, Phys. Rev. E **51**, 4503 (1995).
- [28] L. D. Landau and E. M. Lifshitz, *Theory of Elasticity*, 3rd. ed. (Pergamon, Oxford, 1986).
- [29] J. F. Scott, Rev. Mod. Phys. **46**, 83, (1974).
- [30] Such a treatment has been commonly used in the study of phase transitions in liquid crystals using density wave theory, see for *e.g* Y. Singh, Phys. Rev. A **30**, 583 (1984); M. C. Mahato, M. R. Lakshmi, R. Pandit and H. R. Krishnamurthy, Phys. Rev. A **38**, 1049 (1988).
- [31] R. Biswas and D. Hamann, Phys. Rev. B **36**, 6434 (1987).

FIGURES

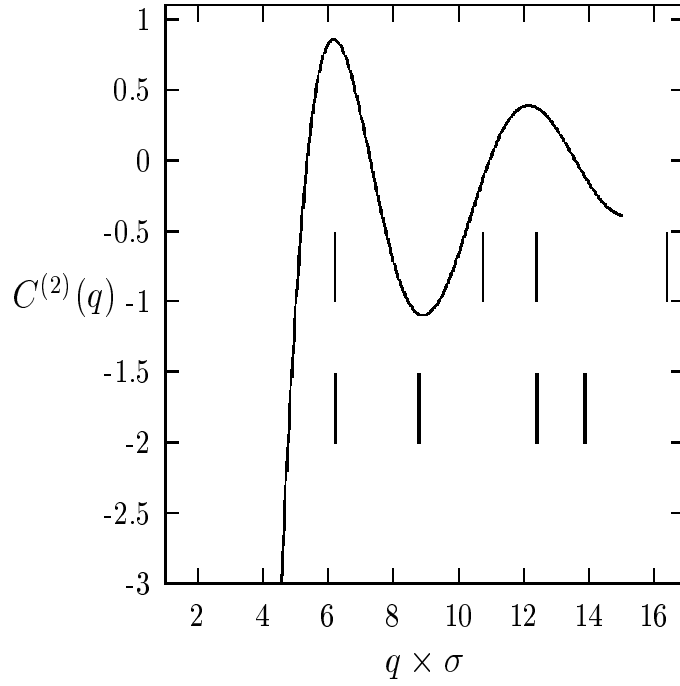


FIG. 1. Plot of the second order direct correlation function  $C^{(2)}(q)$  vs. wavenumber  $q$  for a supercooled hard disk liquid in two-dimensions. The lines mark the lengths of the reciprocal lattice vectors for the triangular (top) and the square (bottom) lattices scaled so that the smallest RLV corresponds to the first peak in  $C^{(2)}(q)$ .

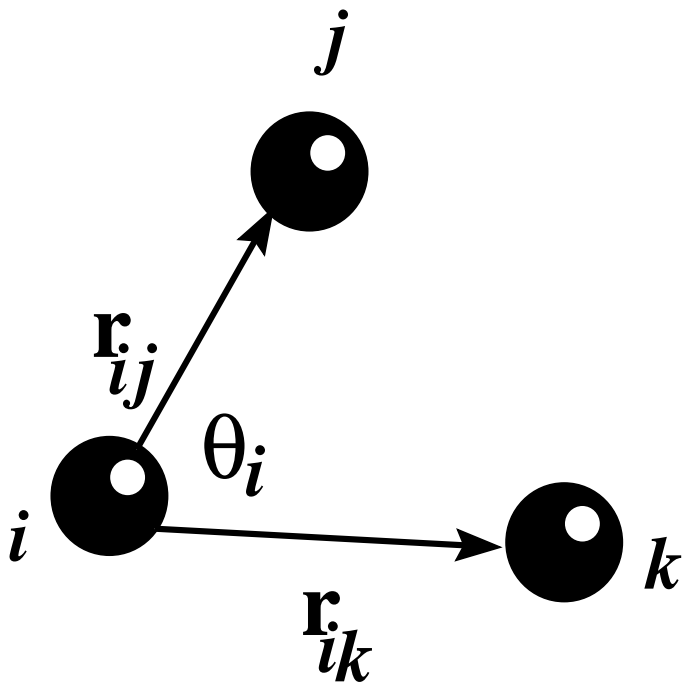


FIG. 2. Definition of angles and distances used in the 3-body potential.

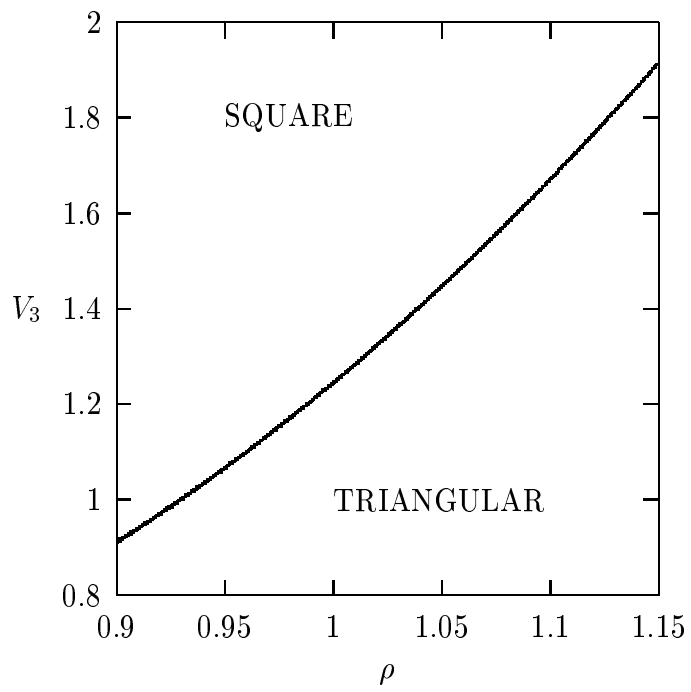


FIG. 3. Zero temperature phase diagram in the  $V_3 - \rho$  plane. The regions where the square and the triangular phases are stable are labelled.



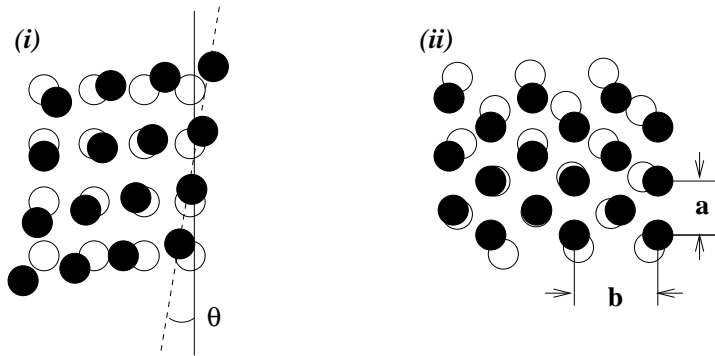


FIG. 4. Two equivalent ways of obtaining a triangular lattice (filled circles) from a square (i) and (ii). One can either (i) shear the original lattice by an angle  $\theta$  or (ii) rotate the original lattice by  $45^\circ$  and then stretch it along one of the axes and compress it along the other so that  $b/a > 1$ . For a square lattice  $\theta = 0, b/a = 1$  and  $\theta = 15^\circ, b/a = \sqrt{3}$  for the ideal triangular lattice. In terms of the shear strain  $\epsilon_3$  the corresponding numbers are 0 and .27812.

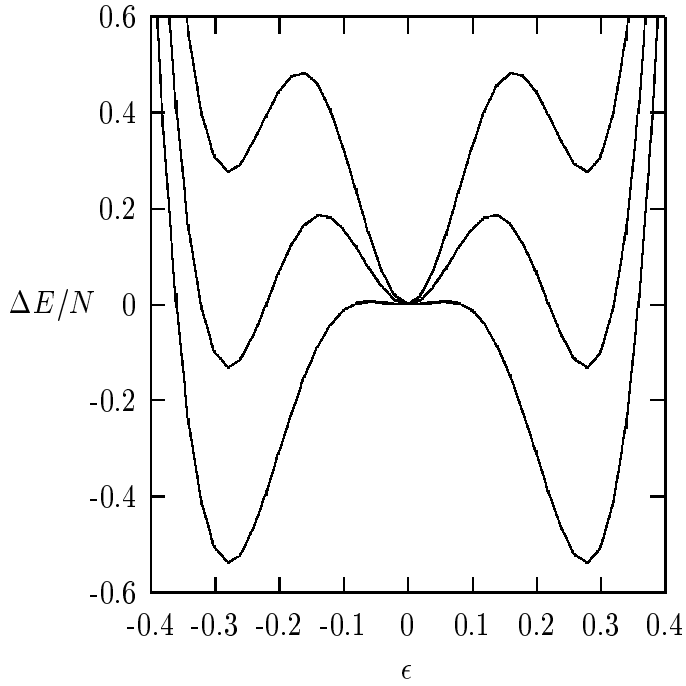


FIG. 5. Energy difference per particle ( $\Delta E/N$ ) between the square and rhombic lattices as a function of the strain order parameter  $\epsilon$  (see text). Of the three minima shown, the one at  $\epsilon = 0$  corresponds to the square phase and the two degenerate minima at  $\epsilon = \pm\epsilon_0$  corresponds to two different orientations of the triangular phase. The curves are for  $V_3 = 2.0$  (top), 1.5 and 1.0. Note the first order transition from the square to the triangular phase as  $V_3$  is reduced.

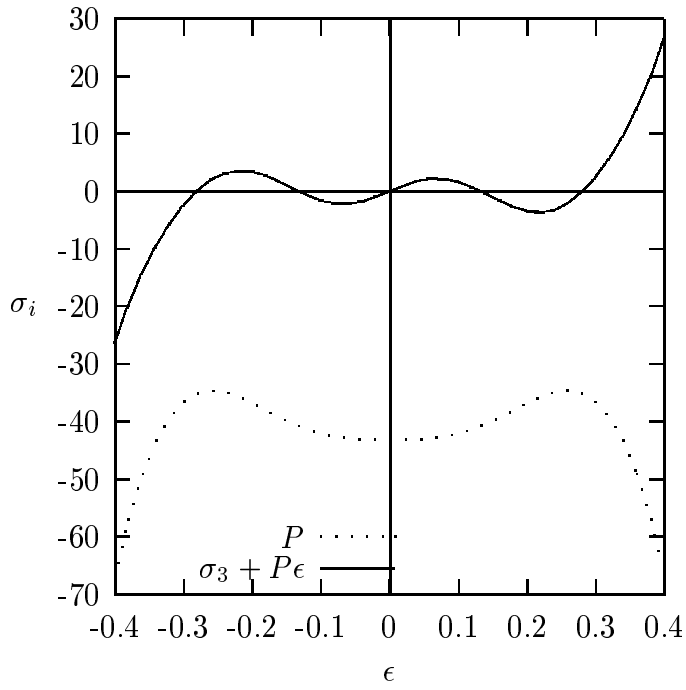


FIG. 6. The pressure  $P = \sigma_1$  and the “effective” shear stress  $\partial E / \partial \epsilon = \sigma_3 + P\epsilon$  as a function of  $\epsilon$  for  $\rho = 1.1$  and  $V_3 = 1.5$ .

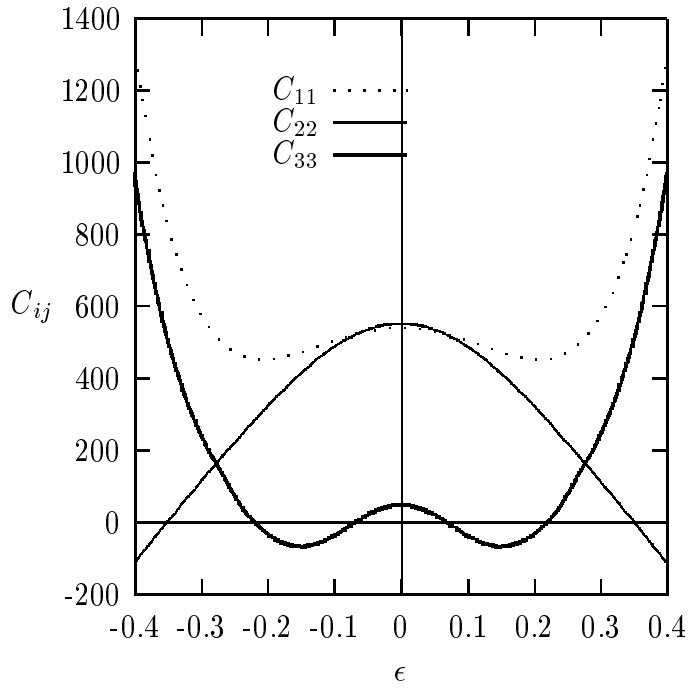


FIG. 7. The  $2^{nd}$  order elastic moduli  $C_{11}$  (bulk),  $C_{22}$  and  $C_{33} + P$  (shear) as a function of  $\epsilon$ . Note that for the triangular lattice  $C_{22} = C_{33} + P$  as required by symmetry. The density  $\rho = 1.1$  and  $V_3 = 1.5$

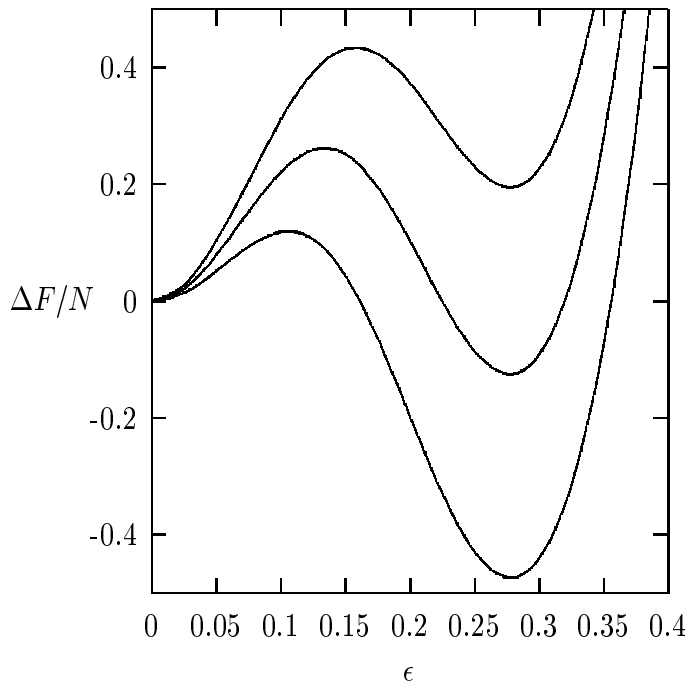


FIG. 8. The per particle Helmholtz free energy difference ( $\Delta F/N$ ) between the square ( $\langle \epsilon \rangle = 0$ ) and rhombic lattices as a function of  $\langle \epsilon \rangle$  for various temperatures  $T = .1$  (top),  $.5$  and  $.1$ . Note the first order phase transition from square to triangular with increasing temperature.

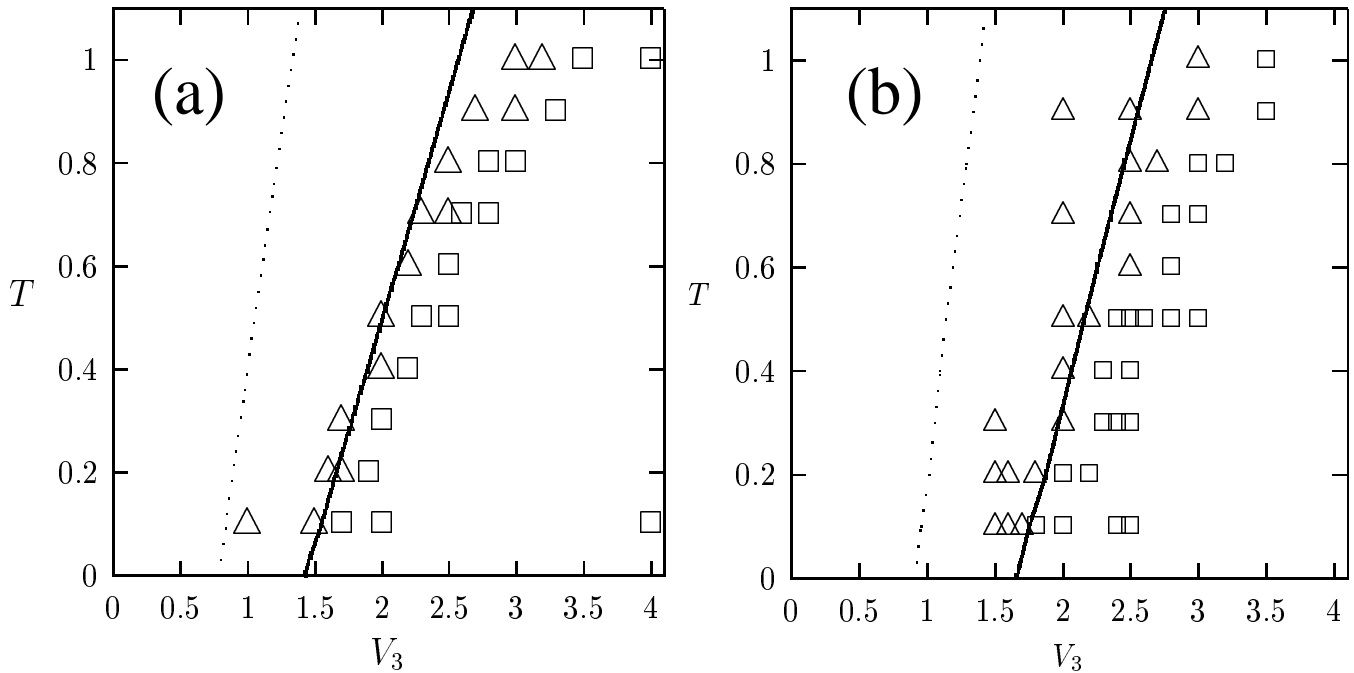


FIG. 9. Phase diagram in the  $T - V_3$  plane for  $\rho = 1.05$  (a) and 1.1 (b). For large  $V_3$  the square phase is stable while the triangular phase is stable for smaller values of  $V_3$ . The points are results from our molecular dynamics simulations in the  $NVT$  ensemble with 2499 particles. Starting from an initial ideal square lattice the system was equilibrated for upto 60000 steps and the final structure noted ( $\square$  for square and  $\Delta$  for triangular) for various values of  $T$  and  $V_3$ . The solid line is the phase boundary resulting from the cell model approximation (see text) and the dashed line is the metastability limit for the square phase from the same theory.

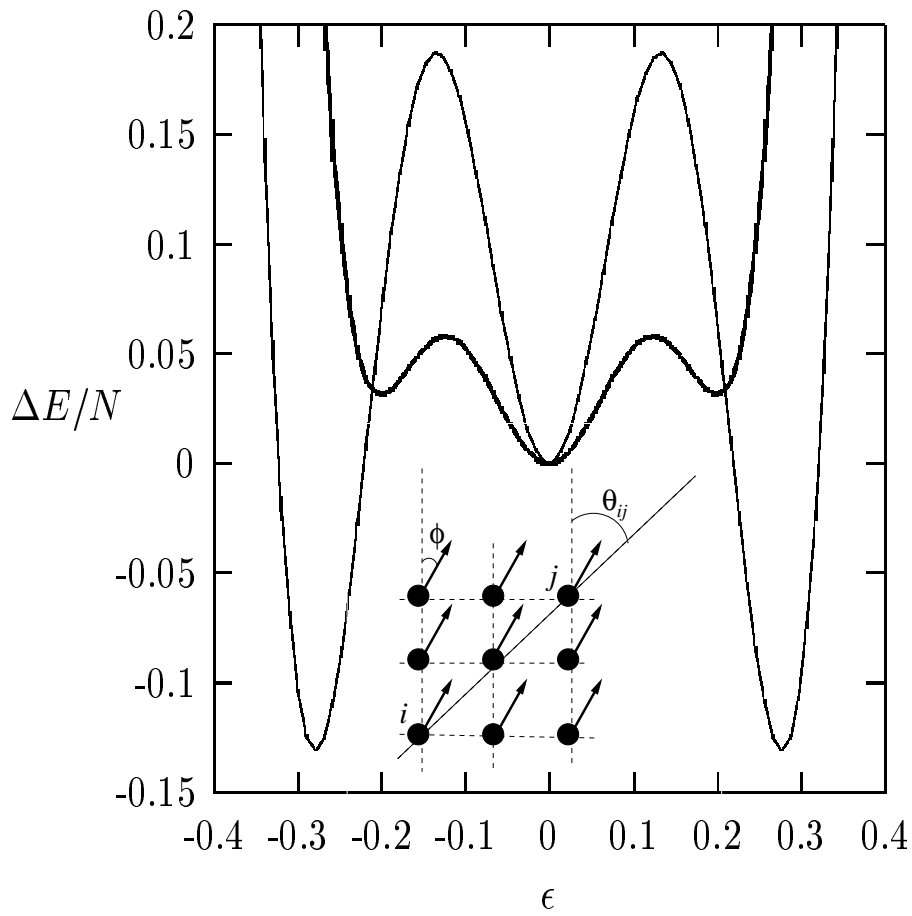


FIG. 10. The energy difference  $\Delta E/N$  for two values of the anisotropy parameter  $\alpha = 0$  and 1 for  $V_3 = 1$  and  $\rho = 1.1$ . Note that the energy minima for  $\epsilon \neq 0$  shifts to lower values of  $\epsilon$  as  $\alpha$  increases. (inset) The meanings of the angles  $\theta_{ij}$  and  $\phi$  used in the text. While  $\theta_{ij}$  is the angle of the position vector  $\mathbf{r}_{ij}$  between the molecules  $i$  and  $j$  measured with respect to the crystal axis  $\{01\}$  in the reference square lattice,  $\phi$  is the orientation of the basis molecule measured with respect to the same axis.

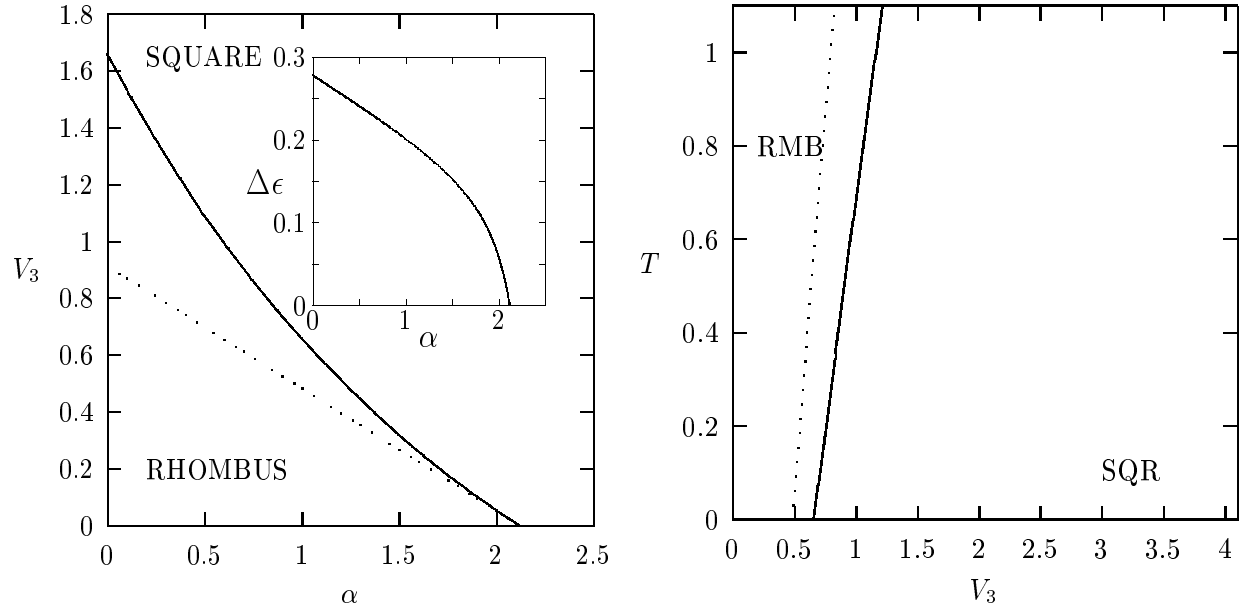


FIG. 11. (left) The zero temperature phase diagram in the  $V_3 - \alpha$  plane for  $\rho = 1.1$ . The dashed line marks the limit of metastability of the square phase. Note that for  $V_3 = 0$  reducing  $\alpha$  produces a second order transition with a tricritical point at  $\alpha_{tc} = 2.24$ . The inset shows the jump in the order parameter  $\Delta\epsilon$  across the square -rhombus phase boundary as a function of the anisotropy  $\alpha$ . (right) The phase diagram in the  $V_3 - T$  plane for  $\alpha = 1$  and  $\rho = 1.1$ . The dashed line marks the limit of metastability of the square phase. Note that in real systems  $\alpha$  depends on  $T$  so that, in general, any quench traverses a trajectory in the parameter space  $T - \alpha - V_3$  and the first-order line may end in a non-zero temperature tricritical point.